Spectrochimica Acta Part A: Molecular and Biomolecular Spectroscopy 150 (2015) 381–389

Contents lists available at ScienceDirect

Spectrochimica Acta Part A: Molecular and Biomolecular Spectroscopy

journal homepage: www.elsevier.com/locate/saa

Vibrational and structural study of onopordopicrin based on the FTIR spectrum and DFT calculations

Fernando E. Chain [a], Elida Romano [b], Patricio Leyton [c], Carolina Paipa [d], César A.N. Catalán [a], Mario Fortuna [e], Silvia Antonia Brandán [b,*]

[a] INQUINOA-CONICET, Instituto de Química Orgánica, Facultad de Bioquímica Química y Farmacia, Universidad Nacional de Tucumán, Ayacucho 471, 4000 S.M. de Tucumán, Tucumán, Argentina
[b] Cátedra de Química General, Instituto de Química Inorgánica, Facultad de Bioquímica, Química y Farmacia, Universidad Nacional de Tucumán, Ayacucho 471, 4000 San Miguel de Tucumán, Tucumán, Argentina
[c] Instituto de Química, Pontificia Universidad Católica de Valparaíso, Valparaíso, Chile
[d] Departamento de Ciencias Químicas, Facultad de Ciencias Exactas, Universidad Andrés Bello (UNAB), Quillota 910, Viña del Mar, Chile
[e] Cátedra de Química Orgánica, Dpto. Cs. Básicas, Facultad de Agronomía y Zootecnia, Universidad Nacional de Tucumán, Av. Néstor Kirchner, 4000 San Miguel de Tucumán, Tucumán, Argentina

HIGHLIGHTS

- Onopordopicrin was studied by infrared and NMR spectroscopies.
- The complete assignment of the vibrational spectra was performed.
- NMR spectra were successfully compared with the calculated chemical shifts.
- The electronic delocalizations were evaluated by means of NBO analysis.
- Some descriptors were predicted by using the HOMO–LUMO studies.

GRAPHICAL ABSTRACT

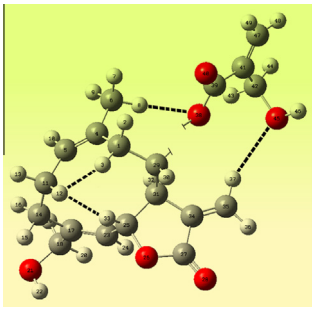

ARTICLE INFO

Article history:
Received 19 January 2015
Received in revised form 2 May 2015
Accepted 23 May 2015
Available online 29 May 2015

Keywords:
Onopordopicrin
Vibrational spectra
Molecular structure
Force field
DFT calculations

ABSTRACT

In the present work, the structural and vibrational properties of the sesquiterpene lactone onopordopicrin (OP) were studied by using infrared spectroscopy and density functional theory (DFT) calculations together with the 6-31G* basis set. The harmonic vibrational wavenumbers for the optimized geometry were calculated at the same level of theory. The complete assignment of the observed bands in the infrared spectrum was performed by combining the DFT calculations with Pulay's scaled quantum mechanical force field (SQMFF) methodology. The comparison between the theoretical and experimental infrared spectrum demonstrated good agreement. Then, the results were used to predict the Raman spectrum. Additionally, the structural properties of OP, such as atomic charges, bond orders, molecular electrostatic potentials, characteristics of electronic delocalization and topological properties of the electronic charge density were evaluated by natural bond orbital (NBO), atoms in molecules (AIM) and frontier orbitals studies. The calculated energy band gap and the chemical potential (μ), electronegativity (χ), global hardness (η), global softness (S) and global electrophilicity index (ω) descriptors predicted for OP low reactivity, higher stability and lower electrophilicity index as compared with the sesquiterpene lactone cnicin containing similar rings.

* Corresponding author. Tel.: +54 381 4247752; fax: +54 381 4248169.
E-mail address: sbrandan@fbqf.unt.edu.ar (S.A. Brandán).

http://dx.doi.org/10.1016/j.saa.2015.05.072
1386-1425/

Introduction

As part of our investigations on compounds that contain rings in their structures and exhibit important biological activities [1–13], in this work, we studied the structural and vibrational properties of onopordopicrin (OP), a sesquiterpene lactone isolated from the weed *Centaurea tweediei*. Onopordopicrin exhibits antimicrobial and cytotoxic activities, especially against human-derived macrophages [14] and against epidermoid carcinoma cells [15]. To date, the molecular structure of OP has not been reported, and there is little information that has been gathered concerning this compound by theoretical studies of its geometry and vibrational spectra. From a chemical point of view, it is known that OP is isolated as oil, and its geometrical parameters have been compared with those of another sesquiterpenoid, costunolide, which has a common basic structure [16]. Due to its significant pharmacological bioactivity, it is of great interest to carry out structural and vibrational studies of this compound. Hence, an experimental and theoretical study of OP combining FT-IR spectroscopy with DFT calculations was performed to understand the stable structure that produces the experimentally observed infrared spectrum and thus carry out complete assignments of the observed bands to the vibration normal modes. For this purpose, the internal normal coordinate's analysis was accomplished with the generalized valence force field (GVFF) by using the SQM methodology [17]. Then, the results were used to predict the Raman spectrum of OP. We demonstrated that the molecular force field for the compound, calculated by using the B3LYP/6-31G* combination, can be well-described. Additionally, the structural properties of OP, such as atomic charges, bond orders, molecular electrostatic potentials, characteristics of electronic delocalization and topological properties of the electronic charge density, were evaluated by NBO [18], AIM [19,20] and HOMO–LUMO studies. The reactivity and behavior of OP were predicted by using some descriptors reported in the literature [13]. Here, the comparisons between the topological properties, the frontier orbitals and useful descriptors for OP with those calculated in this work for other sesquiterpene lactone containing similar rings such as, cnicin show that the presence of a higher quantity of OH groups in cnicin justifies the increase in their reactivity, as compared with OP. We think that this work constitutes a very important insight to understand the connection existent between the different chemical groups present in onopordopicrin in relation to their biological properties.

Experimental methods

Onopordopicrin was isolated from a chloroform extract of the aerial parts of *C. tweediei*, according to the protocol of Bach et al. [14,21]. The FTIR spectrum of the compound in the region of 4000–400 cm^{-1} was recorded between KBr windows with a Fourier Transform Infrared (FT-IR) Perkin Elmer Spectrum RX spectrometer equipped with a DTGS (deuterated triglycine sulfate) detector. The spectral resolution was 4 cm^{-1} and 16 scans were performed. It was not possible to obtain the Raman spectrum of the sample due to interference with the laser line.

Oil; m/z (% relative intensity) (HR-EIMS; [M+] m/z 333.0128): [α]α + 27.70 (0.062; MeOH).

Computational details

The initial geometry of OP was modeled with the *GaussView* program [22] and optimized at the B3LYP/6-31G* level of theory by using the Gaussian program [23]. The potential energy curves described by the C29–O38–C39–C41, C39–C41–C42–O45, C41–C42–O45–H46, C17–C18–O21–H22, C29–O38–C39–O40 and C14–C17–C18–O21 dihedral angles show a total of nineteen configurations with minima energies. Here, we have considered only that conformation with bigger population analysis (99.99%), as indicated in Table S1 (Supporting material) and, in agree with that experimental absolute configuration reported by Droźdź et al. for onopordopicrin by means infrared and NMR studies [24]. The corresponding geometrical parameters for the ten member's ring are similar to the sesquiterpene lactone cnicin [25]. Thus, the most stable structure with C_1 symmetry together with labeled atoms and a stereographic projection of the compound can be observed in Fig. 1. The predicted H-bonds are indicated by dashed lines. Natural charges (NPA) and bond orders were also calculated at the same level of theory for the stable OP structure from the NBO calculation by using the NBO 3.1 program [26], as implemented in the Gaussian 09 program [23]. The molecular electrostatic potentials (MEP) were calculated at the same level of approximation employing Merz–Kollman charges (MK) [27] whereas the surface MEP mapped was produced using the *GaussView* program [22]. The topological analysis of the compound was performed by using the AIM2000 program [20]. The harmonic force field for the compound was evaluated at the B3LYP/6-31G* level following the SQMFF procedure [28]; the potential energy distribution (PED) components ⩾ 10% were subsequently calculated using the SQM results. The natural internal coordinates for OP were defined according to those reported in the literature for similar molecules [1,9,11,12]; these coordinates are listed in Table S2. The MOLVIB program [29,30] was used to transform the resulting force field into "natural" internal coordinates. The nature of all of the vibration normal modes was also analyzed by the *GaussView* program [22]. Here, the Raman spectrum of OP was predicted at the B3LYP/6-31G* level of theory. The calculated ^{1}H NMR and ^{13}C NMR chemical shifts for OP were obtained

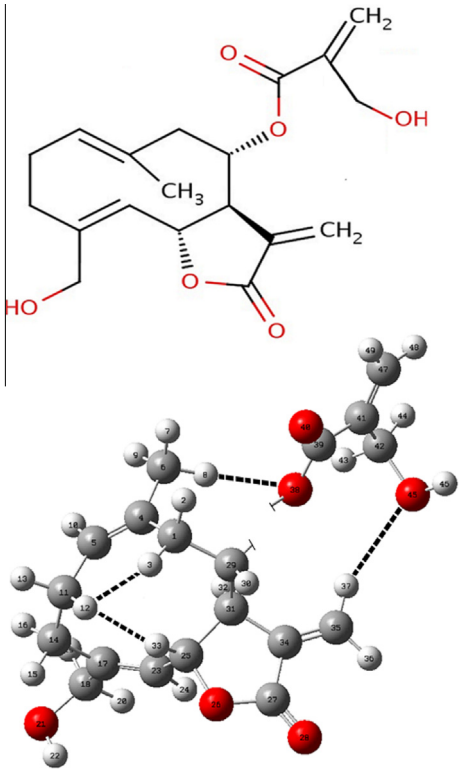

Fig. 1. (a) Stereographic projection of the most stable structure of onopordopicrin and (b) Theoretical structure and atoms numbering. The H-bondings are indicated by dashed lines.

Table 1
Calculated geometrical parameters for onopordopicrin.

Parameter	[a]6-31G*	[b]Exp.
Bond length (Å)		
C39–O40	1.214	
C27–O28	1.206	1.204 (3)
C18–O21	1.427	
C42–O45	1.428	
C25–O26	1.455	1.473 (2)
C27–O26	1.366	1.348 (2)
C29–O38	1.455	
C39–O38	1.354	
C1–C4	1.516	1.500 (3)
C1–C29	1.547	1.546 (3)
C4–C5	1.343	1.326 (3)
C4–C6	1.512	1.496 (3)
C5–C11	1.505	1.485 (3)
C11–C14	1.548	1.555 (3)
C14–C17	1.523	1.512 (3)
C17–C23	1.342	1.329 (2)
C17–C18	1.518	1.487 (3)
C23–C25	1.503	1.483 (2)
C25–C31	1.565	1.544 (2)
C31–C29	1.543	1.536 (2)
C31–C34	1.511	1.506 (2)
C34–C27	1.492	1.483 (3)
C34–C35	1.335	1.315 (3)
O21–H22	0.971	
O45–H46	0.971	
RMSD[b]	0.093	
Bond angle (°)		
C18–O21–H22	106.9	
C42–O45–H46	107.4	
O40–C39–O38	123.8	
O26–C25–C23	108.0	110.8 (1)
O26–C27–O28	122.3	121.7 (2)
O26–C25–C31	106.1	105.2 (1)
O26–C27–C34	108.8	109.1 (1)
O28–C27–C34	128.9	129.2 (2)
C29–O38–C39	117.0	
C25–O26–C27	111.7	110.4 (1)
C23–C25–C31	112.6	113.7 (1)
C11–C14–C17	119.9	108.8 (1)
C14–C11–C5	113.7	109.8 (2)
C14–C17–C18	112.8	117.8 (2)
C14–C17–C23	129.5	117.9 (2)
C17–C23–C25	130.5	126.1 (1)
C18–C17–C23	117.6	123.8 (2)
C25–C31–C34	102.0	101.2 (1)
C27–C34–C31	108.3	107.7 (1)
C27–C34–C35	121.4	120.8 (2)
C29–C31–C25	113.3	116.2 (1)
C29–C31–C34	112.5	114.8 (1)
C1–C29–C31	115.7	117.4 (1)
C1–C4–C5	123.6	121.7 (1)
C1–C4–C6	116.1	114.5 (2)
C5–C4–C6	120.3	123.8 (2)
C4–C5–C11	129.2	127.7 (2)
C4–C1–C29	116.5	114.9 (1)
C31–C34–C35	130.3	131.5 (2)
C42–C41–C47	122.1	
O38–C39–C41	111.9	
RMSD[b]	4.7	
Dihedral angles (°)		
C17–C18–O21–H22	−62.4	
C41–C42–O45–H46	−56.8	
C29–O38–C39–O40	0.2	
C47–C41–C42–O45	108.6	
O26–C25–C23–C17	129.1	110.5 (2)
O26–C25–C31–C29	−103.7	−149.9 (1)
O26–C25–C31–C34	17.4	−24.9 (1)
O26–C27–C34–C31	5.6	−8.5 (2)
O26–C27–C34–C35	−174.7	171.8 (2)
C27–O26–C25–C23	105.5	145.1 (1)
C25–O26–C27–O28	−173.9	172.7 (2)
C1–C4–C5–C11	−0.2	164.6 (2)
C1–C29–C31–C34	−169.5	158.4 (1)
C4–C5–C11–C14	−125.2	−101.8 (2)
C11–C5–C4–C6	178.8	−13.6 (3)
C11–C14–C17–C18	−148.6	82.9 (2)
C11–C14–C17–C23	−33.8	−88.6 (2)
C14–C17–C23–C25	−1.9	155.9 (2)
C23–C25–C31–C29	138.4	88.6 (2)
C23–C25–C31–C34	−100.5	−146.4 (1)
C25–C31–C29–C1	−54.4	−83.9 (2)
C25–C31–C34–C27	14.0	20.5 (2)
C25–C31–C34–C35	166.4	−159.8 (2)
C25–O26–C27–C34	6.4	−8.6 (2)
C29–C1–C4–C5	108.4	−111.7 (2)
C29–C1–C4–C6	72.9	66.7 (2)
C29–C31–C34–C27	107.7	146.4(1)
C29–C31–C34–C35	−71.9	−33.9 (3)
C31–C29–C1–C4	−44.4	73.6 (2)
C31–C34–C27–O28	173.9	170.0 (2)
C35–C34–C27–O28	5.7	−9.7 (4)
C27–O26–C25–C31	−15.4	21.8 (2)
C5–C11–C14–C17	53.6	52.0 (2)
C18–C17–C23–C25	−179.4	−15.1 (3)
C17–C23–C25–C31	−114.1	−131.2 (2)
C1–C29–O38–C39	87.2	
C41–C39–O38–C29	−178.1	
RMSD[b]	117.9	

[a] This work.
[b] From Ref. [16].

employing the Gauge Independent Atomic Orbital (GIAO) method [31] by using the B3LYP/6-311++G** level of theory because the size of this basis set is recommended for NMR chemical shift calculations [32,33]. The calculations were performed using the geometries optimized for this level of theory and TMS as a reference. The results were compared with experimental NMR data from Ref. [34].

Results and discussion

Geometry optimization

The dipole moment value for the most stable structure of OP obtained by using the B3LYP/6-31G* method is 5.72 D (Table S1). It is important to note that the OP molecule has a certain polarity due to the presence of two O atoms, one of them belonging to the side chain and the other one to the lactone ring; the molecule also possesses two carboxyl and two hydroxyl groups. The direction and position of the dipole moment of OP are shown in Fig. S1. Table 1 shows a comparison of the calculated geometrical parameters obtained for OP by using the B3LYP/6-31G* method, with the experimental values determined by Bovill et al. [16] for costunolide by X-ray diffraction. A comparison between the calculated geometrical parameters values and the available experimental data by the root-mean-square deviation (RMSD), reported in Table 1, indicates a acceptable agreement for the bonds lengths (0.093 Å) and angles (4.7°), whereas for the dihedral angles the correlation is significantly lower (117.9°), as shown in Table 1. The differences observed in the geometrical parameters are attributed to the molecule costunolide because it is slightly different from OP. Thus, the RMSD values for bonds lengths and angles suggest that the optimized OP structure provided a reliable starting point for the frequencies and B3LYP/6-31G* force field calculations.

Atomic charges, bond orders, MEP and NBO studies

To investigate the stability of the most stable conformer of OP, the nature of the different interactions and the potentials

electrophilic and/or nucleophilic sites, atomic natural charges (NPA), bond orders, molecular electrostatic potentials and second-order perturbation energies were investigated by using MK charges and NBO calculations [18]. The NPA charges, bond orders and molecular electrostatic potentials for OP calculated at the B3LYP/6-31G* level of theory are presented in Table S3, whereas the second-order perturbation energies are summarized in Table S4. Fig. S2 shows the mapped surface on the molecular surface of the OP structure. The results show that the stability of OP is associated with the positive and negative high atomic charge values on the C27, C39, C6, O21, O40 and O45 atoms, related to the charge values on the other atoms, whereas high negative molecular electrostatic potential values occur on the O26, O28 and O45 atoms belonging to the OC=O groups. These two regions are potential nucleophilic sites, and thus, strong red colorations are expected on these two hydrogen bond acceptor regions, as can be seen in Fig. S2. On the contrary, the less negative molecular electrostatic potential values are observed on the H22 and H46 atoms belonging to the two OH groups, thus, these potential electrophilic sites are H bond donors, with the O45–H46 bond constituting the strongest H bond donor group, as we will see later.

The second-order perturbation energies $E^{(2)}$ (donor → acceptor) that involve the most important delocalization for OP calculated by using the 6-31G* basis set are presented in Table S4. The results show clearly that the contributions of the stabilization energies to the $\Delta ET_{n\rightarrow\pi^*}$ and $\Delta ET_{n\rightarrow\sigma^*}$ charge transfers, due mainly to the lone electron pairs of the O atoms are higher than the remaining delocalizations observed in Table S4. On the other hand, another important $\Delta ET_{\pi^*\rightarrow\pi^*}$ delocalization attributed to the C27=O28 double bond has a higher value than the $\Delta ET_{\pi\rightarrow\sigma^*}$ charge transfer attributed to the C39=O40 double bond. Thus, the total energy values evidently reveal the high stability of OP due mainly to the two ketone functional groups and to the presence of oxygen atoms in the overall structure.

AIM analysis

To elucidate the magnitude of the different interactions present in OP are useful the calculations of the topological properties, such as the calculated electronic charge density $\rho(r)$ and the *Laplacian* values $\nabla^2\rho(r)$ in the bond critical points (BCPs) and in the ring critical points (RCPs). Thus, these properties were calculated for OP by using the AIM2000 program [20] and the B3LYP/6-31G* method. The results can be seen in Table S5. The BCPs are characterized by a closed–shell interaction; it is, the value of $\rho(r)$ is relatively low, the $|\lambda 1|/\lambda 3$ ratio is <1 and $\nabla^2\rho(r)$ is positive, indicating that the interaction is dominated by charge contraction away from the interatomic surface toward each nucleus. Details of the molecular model for onopordopicrin showing the geometry of all the BCPs and RCPs are presented in Fig. S3. This analysis clearly shows (i) four different BCPs, including two O---H bonds and two H---H bonds interactions, and (ii) six RCPs, which are visibly indicated in Table S5. Note that the topological properties of the two H---H bonds interactions present higher values due to the proximity between both atoms involved in the H bond formation, as indicated in Table S5. Thus, these two types of interactions are the most important in this molecule justifying, this way, the high stability of OP. When, the topological properties obtained for OP are compared with those obtained for cnicin, whose structure has one ring of five members (A5) and other of ten members (A10), a higher number of BCPs and RCPs are obtained, as reported in the literature [25].

NMR analysis

Experimental available data from Ref. [34] and chemical shifts calculated for the ^{1}H and ^{13}C nuclei by using the GIAO method [31] are compared in Tables S6 and S7, respectively. Chemical shifts calculated for H nuclei show a good correlation with respect to the experimental values (RMSD 0.072 and 0.096 ppm), whereas the chemical shifts for carbon nuclei show higher deviations (9.4 and 10.6 ppm, respectively) [15,24]. Note that in general the calculated shifts for the ^{13}C nuclei are smaller than the corresponding experimental values, as observed in similar compounds [11,12]. A very important result is that the theoretical calculations predict the chemical shifts values for the H22 and H46 nuclei belonging to the OH groups, as observed in Table S6, but experimentally the corresponding chemical shifts were not observed probably because those groups are involved in intra-molecular H bonds, as revealed by the AIM calculations. Table S7 shows that the ^{13}C chemical shifts calculated with the GIAO method using the 6-311++G** basis set do not agree as well with the experimental values, a result also observed in cnicin [25].

Vibrational analysis

Comparison of the recorded infrared spectrum for OP with the corresponding theoretical scaled can be observed in Fig. 2 while

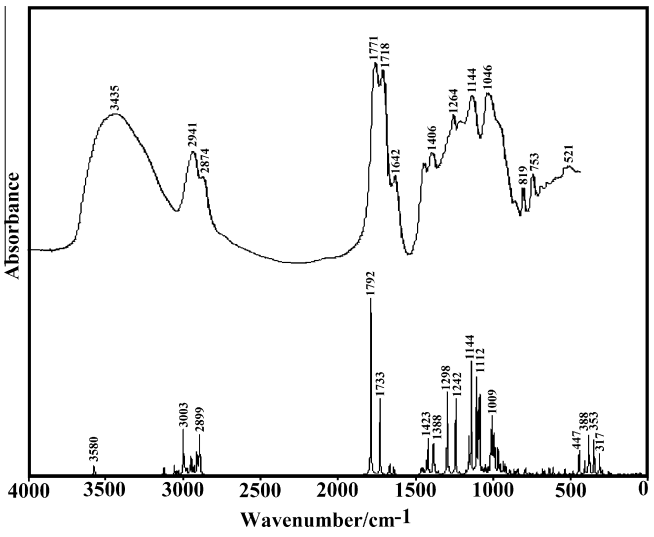

Fig. 2. Experimental infrared spectrum of onopordopicrin (upper) compared with the corresponding scaled theoretical at B3LYP/6-31G* level of theory (bottom).

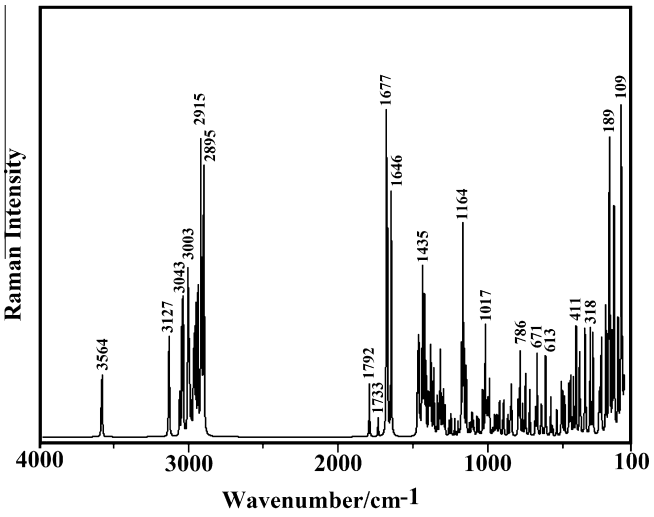

Fig. 3. Predicted Raman spectrum of onopordopicrin at B3LYP/6-31G* level of theory corrected according to Refs. [35,36].

Table 2
Observed and calculated wavenumbers (cm^{-1}) and assignment for onopordopicrin.

Mode	IR[a] Solid	Calc.[b]	SQM[c]	IR int.[d]	Raman int.[d]	Assignment[a]
1	3435 s	3735	3580	53.9	0.02	ν(O45–H46)
2	3435 s	3729	3575	333.6	0.02	ν(O21–H22)
3	3137 sh	3266	3131	1.2	0.02	ν_{as} = CH_2(C47)
4	3137 sh	3262	3127	3.9	0.03	ν_{as} = CH_2(C35)
5		3190	3059	4.1	0.01	ν(C25–H33)
6		3174	3043	6.1	0.04	ν_s = CH_2(C47)
7		3166	3034	3.6	0.04	ν_s = CH_2(C35)
8		3135	3004	22.1	0.02	$\nu_{as}CH_2$(C42)
9		3133	3003	29.3	0.02	$\nu_{as}CH_2$(C11)
10		3131	3001	11.0	0.03	ν(C23–H24)
11	2994 sh	3125	2996	12.2	0.02	$\nu_{as}CH_3$(C6)
12		3121	2992	18.6	0.02	ν(C5–H10)
13		3113	2984	27.6	0.00	ν(C29–H30)
14		3107	2978	3.4	0.01	$\nu_{as}CH_2$(C1)
15		3094	2966	19.5	0.02	ν(C31–H32)
16		3089	2960	37.3	0.03	$\nu_{as}CH_3$(C6)
17		3078	2951	39.9	0.04	$\nu_{as}CH_2$(C18)
18	2941 m	3065	2938	40.7	0.03	$\nu_{as}CH_2$(C14)
19		3062	2935	80.1	0.04	$\nu_s CH_2$(C1)
20		3042	2916	39.8	0.90	$\nu_s CH_2$(C14)
21		3035	2909	12.9	0.05	$\nu_s CH_3$(C6)
22	2874 m	3025	2899	4.3	0.05	$\nu_s CH_2$(C42)
23	2874 m	3021	2896	22.0	0.04	$\nu_s CH_2$(C18)
24	2874 m	3020	2895	56.5	0.04	$\nu_s CH_2$(C11)
25	1771 vs	1861	1792	384.6	0.02	ν(C27═O28)
26	1718 vs	1799	1733	207.0	0.01	ν(C39═O40); ρCOO
27	1654 m	1743	1677	20.2	1.00	ν(C17═C23); ν(C–C)*ip(2)*
28	1642 m	1742	1674	6.0	0.01	ν(C4═C5)
29	1642 m	1733	1670	20.3	0.06	ν(C34═C35); ν(C–C)*ip(3)*
30	1632 sh	1708	1645	28.2	0.08	ν(C41═C47)
31		1538	1470	0.0	0.02	δCH_2 (C11)
32	1465 sh	1531	1464	3.5	0.01	$\delta_{as}CH_3$ (C6)
33		1530	1462	4.2	0.02	δCH_2 (C18)
34	1452 m	1526	1459	12.6	0.02	δCH_2 (C42)
35		1517	1451	2.5	0.00	δCH_2 (C1)
36	1441 sh	1507	1441	5.5	0.02	$\delta_{as}CH_3$ (C6)
37		1500	1435	8.9	0.03	δCH_2(C14)
38		1474	1434	20.9	0.03	δ = CH_2 (C35)
39		1458	1423	19.0	0.04	δ = CH_2 (C47)
40	1406 m	1446	1413	1.8	0.02	$wagCH_2$ (C18)
41	1397 m	1443	1396	120.3	0.01	ρ′(C29–H30)
42	1397 m	1433	1392	6.7	0.01	$wagCH_2$ (C42)
43		1429	1388	29.2	0.01	$wagCH_2$ (C14)
44	1382 sh	1427	1381	8.2	0.03	δsCH_3(C6)
45		1415	1374	11.2	0.00	β(C23–H24)
46		1402	1363	2.9	0.02	ρ(C29–H30)
47	1352 sh	1398	1358	7.5	0.01	β(C5–H10)
48		1381	1338	1.1	0.01	$wagCH_2$ (C1)
49	1322 sh	1379	1323	4.4	0.01	$wagCH_2$ (C11)
50		1367	1317	1.5	0.03	ρ′(C25–H33)
51		1359	1306	18.4	0.00	δ(O21–H22); τwCH_2(C18)
52		1352	1304	0.7	0.00	δ(O45–H46)
53	1299 sh	1332	1298	32.1	0.01	ρ(C25–H33)
54		1329	1287	220.9	0.01	ν(C41–C42)
55	1264 m	1298	1260	3.2	0.01	ν(C–C)*op(3)*; ρ = CH_2(C35)
56		1295	1246	33.1	0.01	ρ(C31–H32)
57	1224 m	1270	1221	26.5	0.01	ρ′(C31–H32); βR_1 (A10)
58	1199 m	1261	1199	69.4	0.00	ν(C4–C6); βR_6 (A10); ν(C1–C4)
59		1251	1177	21.6	0.02	ν(C39–O38); δCOO
60	1168 sh	1239	1166	30.6	0.05	βR_3 (A10); ν(C–C)*op(2)*; βR_2 (A10)
61		1224	1159	27.1	0.02	ρCH_2 (C14)
62	1144 s	1220	1144	16.4	0.03	ρCH_2(C1)
63	1121 sh	1205	1125	26.2	0.00	ρCH_2 (C11)
64		1199	1112	16.2	0.01	ν(C27–O26); β (C27═O28)
65		1182	1105	252.1	0.00	ρCH_2(C42)
66		1144	1098	110.3	0.01	ρCH_2(C18)
67		1130	1091	23.6	0.00	ν(C5–C11); ρCH_3 (C6)
68	1069 sh	1115	1073	25.1	0.01	ρ′CH_3 (C6)
69		1097	1062	62.9	0.01	ν(C17–C18)
70	1046 s	1084	1051	24.7	0.00	ν(C–C)*op(1)*; ν(C29–C31)
71	1025 s	1069	1035	121.6	0.01	δ(C29C31C34)
72		1060	1019	10.2	0.01	ν(C42–O45)
73		1048	1017	7.2	0.03	δ(O26C25C23)
74		1044	1009	17.9	0.01	wag = CH_2(C35)

(*continued on next page*)

Table 2 (*continued*)

Mode	IR[a] Solid	Calc.[b]	SQM[c]	IR int.[d]	Raman int.[d]	Assignment[a]
75	1006 sh	1036	1005	1.6	0.01	ν(C18–O21); ν(C25–O26)
76		1029	999	7.5	0.01	ν(C11–C14)
77	991 sh	1015	995	59.9	0.00	δ(C29C31C34); βR_5(A10)
78		1006	990	158.3	0.02	wag = CH_2(C47)
79	973 sh	1003	972	29.9	0.00	ν(C–C)*ip(1)*
80		991	967	29.5	0.00	τwCH_2 (C11)
81		984	957	18.3	0.01	τwCH_2 (C42)
82		973	947	17.6	0.01	βR_5 (A10)
83		969	938	19.9	0.01	ρ = CH_2 (C47)
84	926 sh	960	925	8.1	0.01	τwCH_2 (C1)
85		951	921	3.1	0.01	βR_4 (A10)
86		918	898	2.0	0.01	γ(C23–H24)
87		904	894	3.0	0.01	γ(C5–H10)
88	872 w	886	867	5.5	0.01	ν(C29–O38)
89	851 sh	866	850	6.0	0.01	τwCH_2 (C14)
90		861	843	11.6	0.02	δ(C29O38C39)
91	819 w	838	799	9.6	0.01	γ(C27=O28); τw = CH_2 (C35); γ(C34=C35); τR_2 (A5)
92		824	792	22.4	0.01	γ(COO); γ(C41=C47)
93		814	786	1.6	0.02	δ(O26C25C23); τR_2(A10)
94		794	768	18.1	0.01	βR_2 (A5)
95	753 w	777	749	14.2	0.02	βR_4 (A10); δ(C29C31C34)
96		746	721	10.5	0.01	δ(C29C31C34); τR_1 (A5); βR_4 (A10)
97	700 w	732	683	2.7	0.01	τwCH_2 (C47); δ (C41C42O45)
98	666 w	698	671	2.6	0.03	βR_1 (A5); γ(C4–C6)
99		684	644	9.1	0.01	δ(C17C18O21)
100	634 sh	653	640	0.1	0.01	βR_4 (A10); βR_3 (A10); τR_1 (A5)
101	614 vw	625	615	11.2	0.03	βR_1 (A5)
102		601	581	10.2	0.01	ν(C39–C41)
103		588	568	49.3	0.00	δ(O26C25C23)
104	548 w	557	540	55.0	0.01	τR_1 (A5); δ(C29C31C34)
105	509 vw	523	509	45.5	0.02	τR_1 (A5)
106		514	502	58.5	0.01	βR_5 (A10); βR_4 (A10); τR_3(A10)
107	485 w	504	487	11.9	0.01	τR_1 (A5); δ(O26C25C23); βR_4 (A10)
108	463 w	473	460	92.0	0.01	τR_1 (A5); δ (C29C31C34); βR_5 (A10)
109	456 w	462	450	0.6	0.01	τR_3(A10); δ(O26C25C23); τR_1(A10)
110		458	447	0.4	0.02	τR_3(A10)
111	425 vw	443	429	2.4	0.02	τR_3(A10); τR_1(A10)
112	411 vw	420	411	5.2	0.03	βR_4 (A10); δ(O26C25C23); βR_5 (A10)
113		407	388	0.3	0.03	ρ(C41=C47)
114		388	380	2.7	0.01	τR_1(A10); τR_5(A10)
115		384	353	2.3	0.03	β(C4–C6)
116		365	351	6.9	0.01	τ(O21–H22)
117		361	346	1.0	0.01	βR_4 (A10); τR_5(A10); **δ(O38C29C1)**[#]
118		333	317	1.2	0.03	β(C34=C35)
119		320	300	6.3	0.01	τ(O45–H46); δ(C42C41C39); δ(O38C29C31)
120		314	299	0.9	0.02	δ(O26C25C23); τR_1 (A5); τR_5(A10)
121		274	258	4.6	0.01	βR_4 (A10); τR_1(A10); τR_1 (A5)
122		262	251	3.5	0.01	τR_1(A10)
123		252	243	2.3	0.03	τR_1(A10); βR_4 (A10), **β(C17–C18)**[#]
124		210	212	0.9	0.03	βR_4 (A10); τR_1 (A5)
125		208	195	3.1	0.02	δ(C29C31C34); τR_1(A10)
126		197	189	1.3	0.09	τwCH_3 (C6); **γ(C17–C18)**[#]
127		185	184	0.8	0.02	δ(C29C31C34); τR_2(A10); τR_6(A10)
128		176	169	0.4	0.03	τR_3(A10); τR_1 (A5)
129		167	157	1.6	0.06	τR_6(A10)
130		143	131	1.6	0.03	τR_1(A10); τR_5(A10); βR_5 (A10)
131		120		0.4	0.10	**γ(C4–C6)**[#]
132		108	110	0.9	0.08	τR_5(A10); **τ(O21–C18–C17–C)**[#]
133		105	102	1.5	0.02	τR_1 (A5); τR_7(A10); τR_2(A10)
134		85	81	2.4	0.16	τR_1 (A5); τR_2(A10)
135		81	77	0.9	0.18	δ(C29C31C34)
136		61	57	1.8	0.15	τ(COO); τ(CC29O38C39)
137		60	53	2.1	0.16	τR_7(A10); **Butt**[#]
138		55	50	1.7	0.16	τ(CC39O38C29)
139		46	42	0.5	0.26	τR_4(A10)
140		33	31	1.7	0.53	τR_3(A10); τR_6(A10); τR_7(A10)
141		24	24	0.6	1.00	τR_2(A10)
RMSD (cm^{-1})		73.51	18.28			

ν, stretching; δ, scissoring; wag, wagging or out-of plane deformation; ρ, rocking; τ, torsion, twist, twisting; a, antisymmetric; s, symmetric; ip, in-phase; op, out-of-phase; R, ring; five members, (A5); ten members, (A10).

[#] See text. Letter bold, assigned by *GaussView* program [22].

[a] This work.

[b] From B3LYP/6-31G* calculations.

[c] From scaled quantum mechanics force field B3LYP/6-31G*.

[d] Units are km mol^{-1}.

the predicted Raman spectrum at the B3LYP/6-31G* level is observed in Fig. 3. The calculated Raman activities were converted to relative Raman intensities using the relationship derived from the intensity theory of Raman scattering, as reported in the literature [35,36]. Note that in general the calculated spectrum reproduces the experimental spectrum reasonably well. Clearly, the differences observed between both spectra are attributed to the calculations because the anharmonicity was not taken into account in our calculations in the gas phase, whereas in the condensed phase, the forces due to the H bonds are important, as previously analyzed. Furthermore, the broadening of some bands observed in the infrared spectra probably justifies the H bonds predicted by NBO and AIM calculations. The OP structure has C_1 symmetry and 141 normal vibration modes, all active in the infrared and Raman spectra. Table 2 shows the experimental and calculated wavenumbers for the expected normal vibration modes, the SQM based on the 6-31G* basis set and the corresponding assignments. The theoretical calculations reproduce the normal frequencies for OP with initial value of RMSD of 73.51 cm^{-1} while when the SQMFF method is applied using the scaling factors, the final RMSD decrease significantly until 18.28 cm^{-1}, as observed in Table 2. It is necessary to clarify that the presence of wide bands in the infrared spectrum overlaps some bands and in these cases the theoretical frequencies were considered as experimental ones. The infrared frequencies, the infrared and Raman intensities and the potential energy distribution obtained by B3LYP/6-31G* calculations appear in Table S8. Tables 2 and S8 show clearly that the calculated and SQM wavenumbers for some normal vibration modes are closely distributed, and thus, these modes exhibit a lower PED contribution or are not directly observed (such as the frequency calculated at 120 cm^{-1}). Thus, the assignment of the experimental bands to the normal modes of vibration was performed by taking into account PED contributions $\geqslant$10% for some vibration normal modes; for other modes, i.e., those with low contributions and/or that not observed, the assignments were carried out using the *GaussView* program [22]. These vibration normal modes are defined by the following internal coordinates: S_{99} (δ(O38C29C1)), S_{106} (β(C17–C18)), S_{116} (γ(C17–C18)), S_{131} (Butt) and S_{132} (τ(O21–C18–C17–C)) and are represented in bold letter in Table 2. To perform the complete assignment of OP, we took into account the assignments reported for related molecules [1–6,9–12,24,37–39] and the B3LYP/6-31G* level of calculation because the scale factors used are defined for the 6-31G* basis set [28]. Table S1 summarize the scale factors together with the definitions of the natural internal Coordinates for onopordopicrin. Below, a discussion of the assignments of the most important groups is presented.

Bands assignments

OH modes

In accordance to the values reported for similar compounds [1,3–6,9,11,37–39], the broad band observed in the IR spectrum of the compound in the solid phase at 3435 cm^{-1} is easily assigned to the two O–H stretching modes of OP. The OH in-plane deformation modes for both groups are predicted at 1306 and 1304 cm^{-1} and they are observed overlapped by wide and intense bands in that region, whereas the corresponding out-of-plane deformation modes are not observed in the IR experimental spectrum and, for this reason, they were not assigned, because they are predicted by calculation at 351 and 300 cm^{-1}, as indicated in Table 2.

CH_3 modes

The antisymmetric stretching modes of methyl groups are calculated as totally pure modes at 2996 and 2960 cm^{-1} while the corresponding symmetric mode is predicted at 2909 cm^{-1}, hence, they can be assigned to the shoulder and IR band of the medium intensity at 2994 and 2941 cm^{-1}, respectively, as observed in Table 2. The antisymmetric and symmetric CH_3 bending modes are predicted to occur at 1464, 1441 and 1381 cm^{-1} by SQM calculations; hence, they are assigned to those regions. The rocking and twisting modes are assigned as predicted by the calculations and in accordance with the expected regions for similar compounds [11,12,38,39], as observed in Table 2.

CH_2 modes

The vibration stretching modes corresponding to these groups are calculated in the expected regions; thus, the group of IR bands between 3131 and 2895 cm^{-1} region can be easily assigned to stretching modes, as observed in Table 2. An important observation is that for the CH_2 groups with sp^2 C atoms, stretching and wagging modes are predicted by calculations at higher and lower wavenumbers, respectively than those groups with sp^3 C atoms. Thus, all of the deformation modes for these groups are associated with the shoulders and IR bands between 1470 and 1423 cm^{-1}, whereas the wagging modes are predicted to occur between 1413 and 1323 cm^{-1} for those CH_2 groups with sp^3 C atoms and between 1009 and 990 cm^{-1} for the other ones. The rocking and twisting modes are assigned as predicted by calculations, as indicated in Table 2.

CH modes

The C–H stretching modes are predicted to occur in the 3059–2984 cm^{-1} region. The in-plane and out-of-plane deformation modes are predicted to occur in the expected regions reported for similar molecules [1–3,5,6,9–12,38,39]: 1396–1246 and 898–894 cm^{-1}, respectively.

Skeletal modes

The description of the skeletal stretching modes for OP can be observed in Table 2. The very strong IR bands at 1771 and 1718 cm^{-1} are easily assigned to the C=O stretching modes according to the values reported for similar compounds [1,3–6,9,11,38,39]. Note that the Raman intensities of these bands are lower than the expected because the O atoms belonging to the C27=O28 and C39=O40 groups are involved in $\Delta ET_{LP\rightarrow\sigma^*}$ charge transfers, as observed in Table S4. The C=C stretching modes are predicted to occur between 1677 and 1645 cm^{-1}, and due to the proximity of these bands, the IR bands of the medium intensities at 1654 and 1642 cm^{-1} and the shoulder at 1632 cm^{-1} in the IR spectrum are assigned to C=C stretching modes. Here, the C41=C47 stretching mode was assigned to the shoulders in the IR spectrum at 1636 and 1625 cm^{-1}, respectively because this bond is involved in the $\sigma(2)C41–C47 \rightarrow \sigma^*(2)C39–O40$ delocalization, as observed in Table S4. On the other hand, the C–O stretching modes are predicted between 1177 and 886 cm^{-1}, hence, they are clearly assigned to the shoulders and overlapped bands in those region, as shown in Table 2. According to the values previously reported for molecules with similar rings [1–6,9,11,12,37–39] and the values obtained from our theoretical results, the IR bands at 1199 and 1046 cm^{-1} are associated with some C–C stretching modes. The remaining skeletal modes are assigned according to the calculations, as shown in Table 2.

Force field

The force constants for OP were estimated employing the SQM methodology [28] at the B3LYP/6-31G* level of theory by using the Molvib program [29,30], as was previously described in Computational Details. These constants expressed in internal coordinates are shown in Table 3 and they are compared with the

Table 3
Comparison of scaled internal force constants for onopordopicrin.

Force constant	B3LYP/6-31G*	
	Onopordopicrin[a]	Dehydrofukinone[b]
f(νO–H)	7.16	
f(νC=O)	12.30	11.11
$f(\nu C–O)_{Ring}$	4.80	
f (νC–OH)	4.85	
f(νC=C)	9.13	8.46
f(νC–H)	4.96	4.84
$f(\nu CH_2)$	4.90	4.75
$f(\nu CH_3)$	4.82	4.87
$f(\delta CH_2)(sp^2)$	0.45	
$f(\delta CH_2)$(sp3)	0.77	0.73
$f(\delta CH_3)$	0.55	0.55
f(δOH)	0.74	

Units are mdyn $Å^{-1}$ for stretching and stretching/stretching interaction and mdyn Å rad^{-2} for angle deformations.
[a] This work.
[b] From Ref. [12].

values obtained for an eremophilane-derived sesquiterpene ketone, dehydrofukinone [12], by using the same level of theory. Clearly, the lower values observed for the *f(νC=O)*, *f(νC=C)*, *f(νC–H)* and *f(νCH₂)* force constants for dehydrofukinone are justified because the number of those groups present in the molecule's structure is lower than that observed in the OP structure. For OP, the *f(νC–O)* force constants belonging to the C–O ring and to the side chain were analyzed separately from those corresponding to the C–OH groups but, the calculation show that the obtained values are approximately the same. Furthermore, the force constants corresponding to the CH_2 bending modes assume different values when the C atoms of these groups are sp^2 hybridized than when those groups are sp^3 hybridized. Thus, in the first case, the average value is slightly lower, as observed in Table 3. This difference in the force constants values are justified probably because the bond angles values for the $=CH_2$ groups are between 118.4° and 117.8° while for the other ones the values are among 105.1° and 107.6°.

HOMO–LUMO

To study the reactivity of OP and to predict its behavior in the gas phase, the frontier HOMO–LUMO molecular orbitals and the chemical potential (μ), electronegativity (χ), global hardness (η), global softness (S) and global electrophilicity index (ω) descriptors [13,40–42] were calculated at the B3LYP/6-31G* level of theory. The gap energy band and the descriptors for OP can be observed in Table S9 and are compared with the values obtained in this work for the more stable conformer of cnicin and with those reported in the literature for the C3 conformer of thymidine because it has antiviral property. Comparing the energy band gap of OP (−5.0523 eV) with that obtained for the more stable conformer of cnicin (−4.8217) and thymidine (−5.4748 eV), we observed that OP is less reactive than cnicin but more reactive than thymidine while cnicin is less stable than OP and thymidine because it has a lower η. On the other hand, OP has a better capability for accepting electrons because it has a greater electrophilicity index (3.3505 eV) than thymidine (2.0728 eV) but lower than cnicin (3.5434). In contrast, thymidine is a better electron donor than OP because it is supported by two OH and C=O groups, one NH group, two N atoms and one O atom, whereas OP has two OH and C=O groups and only two O atoms. These studies show clearly that the presence of various OH groups in the cnicin structure increase their reactivity as compared with OP.

Conclusions

In the present work, onopordopicrin was isolated and characterized by using infrared and ^1H, ^{13}C NMR spectroscopies. The theoretical molecular structure for the most stable structure of onopordopicrin was determined by the B3LYP/6-31G* method. NBO and AIM calculations reveal that the high stability of onopordopicrin is due to the hyperconjugation between electron-donating groups, which exhibit high energy values due to the $\Delta ET_{\pi\to\pi^*}$, $\Delta ET_{\pi^*\to\pi^*}$ and $\Delta ET_{n\to\pi^*}$ charge transfers. The AIM study reveals the formation of two O–H intramolecular hydrogen bonds, which may also be responsible for the high stability of onopordopicrin. A complete assignment of the 141 normal vibration modes of the molecule was performed. The SQM force field was obtained, and the theoretical vibrational calculations allowed us to obtain a set of scaled force constants fitting the observed wavenumber values. The calculations of the frontier orbitals and of some descriptors indicate that OP has a lower energy band gap, lower η and a larger electrophilicity index than the potentially antiviral thymidine but the comparison of these descriptors with those calculated for a compound with similar ring in their structure such as, cnicin, show clearly that the presence of higher OH groups in a structure is a structural requirements important for increase the reactivity and the electrophilic index and, for these reasons, their activity.

Acknowledgments

This work was supported by Grants from CIUNT (Consejo de Investigaciones, Universidad Nacional de Tucumán) and CONICET (Consejo Nacional de Investigaciones Científicas y Técnicas, R. Argentina). The authors thank Prof. Tom Sundius for his permission to use MOLVIB. Project DI-125-790-2014 from VRIEA (Vicerrectoria de Investigación y Estudios Avanzados) – PUCV (Pontificia Universidad Católica de Valparaíso) is also acknowledged.

Appendix A. Supplementary data

Supplementary data associated with this article can be found, in the online version, at http://dx.doi.org/10.1016/j.saa.2015.05.072.

References

[1] G.R. Argañaraz, E. Romano, J. Zinczuk, S.A. Brandán, J. Chem. Chem. Eng. 5 (2011) 747–758.
[2] C.D. Contreras, M. Montejo, J.J. Lopez Gonzalez, J. Zinczuk, S.A. Brandán, J. Raman Spectrosc. 42 (1) (2011) 108–116.
[3] E. Romano, A.B. Raschi, A. Benavente, S.A. Brandán, Spectrochim. Acta Part A 84 (2011) 111–116.
[4] E. Romano, M.V. Castillo, J.L. Pergomet, J. Zinczuk, S.A. Brandán, J. Mol. Struct. 1018 (2012) 149–155.
[5] P. Leyton, J. Brunet, V. Silva, C. Paipa, M.V. Castillo, S.A. Brandán, Spectrochim. Acta Part A 88 (2012) 162–170.
[6] S.A. Brandán, F. Marquez Lopez, M. Montejo, J.J. Lopez Gonzalez, A. Ben Altabef, Spectrochim. Acta Part A 75 (2010) 1422–1434.
[7] E. Romano, N.A.J. Soria, R. Rudyk, S.A. Brandán, Mol. Simul. 38 (7) (2012) 561–566.
[8] A. Brizuela, E. Romano, A. Yurquina, S. Locatelli, S.A. Brandán, Spectrochim. Acta Part A Mol. Biomol. Spectrosc. 95 (2012) 399–406.
[9] P. Leyton, C. Paipa, A. Berrios, A. Zárate, S. Fuentes, M.V. Castillo, S.A. Brandán, J. Mol. Struct. 1031 (2013) 110–118.
[10] M.V. Castillo, E. Romano, A.B. Raschi, A. Yurquina, S.A. Brandán, Comput. Theor. Chem. 995 (2012) 43–48.
[11] E. Lizarraga, E. Romano, R.A. Rudyk, C.A.N. Catalán, S.A. Brandán, Spectrochim. Acta Part A Mol. Biomol. Spectrosc. 97 (2012) 202–208.
[12] E. Lizarraga, E. Romano, A.B. Raschi, P. Leyton, C. Paipa, C.A.N. Catalán, S.A. Brandán, J. Mol. Struct. 1048 (2013) 331–338.
[13] D. Romani, S.A. Brandán, Comput. Theoret. Chem. (Theochem) 1061 (2015) 89–99.
[14] S.M. Bach, M.A. Fortuna, R. Attarian, J.T. de Trimarco, C.A. Catalán, Y. Av-Gay, H. Bach, Nat. Prod. Commun. 6 (2) (2011) 163–166.
[15] G. Lonergan, E. Routsi, T. Georgiadis, G. Agelis, J. Hondrelis, J. Matsoukas, L.K. Larsen, F.R. Caplan, J. Nat. Prod. 55 (1992) 225–228.

[16] M.J. Bovill, P.J. Cox, P.D. Cradwick, M.H.P. Guy, G.A. Sim, D.N.J. White, Acta Cryst. B32 (1976) 3203–3209.
[17] P. Pulay, G. Fogarasi, F. Pang, E. Boggs, J. Am. Chem. Soc. 101 (10) (1979) 2550–2560.
[18] A.E. Reed, L.A. Curtis, F. Weinhold, Chem. Rev. 88 (6) (1988) 899–926.
[19] R.F.W. Bader, Atoms in Molecules, A Quantum Theory, Oxford University Press, Oxford, 1990, ISBN 0198558651.
[20] F. Biegler-Koning, J. Schonbohm, D. Bayles, J. Comput. Chem. 22 (2001) 545–559.
[21] A.M. Fortuna, E.C. Riscala, C.A.N. Catalán, T.E. Gedris, W. Herz, Biochem. Syst. Ecol. 29 (2001) 967–971.
[22] A.B. Nielsen, A.J. Holder, Gauss View 3.0, User's Reference, GAUSSIAN Inc., Pittsburgh, PA, 2000–2003.
[23] M.J. Frisch, G.W. Trucks, H.B. Schlegel, G.E. Scuseria, M.A. Robb, J.R. Cheeseman, J.A. Montgomery Jr., T. Vreven, K.N. Kudin, J.C. Burant, J.M. Millam, S.S. Iyengar, J. Tomasi, V. Barone, B. Mennucci, M. Cossi, G. Scalmani, N. Rega, G.A. Petersson, H. Nakatsuji, M. Hada, M. Ehara, K. Toyota, R. Fukuda, J. Hasegawa, M. Ishida, T. Nakajima, Y. Honda, O. Kitao, H. Nakai, M. Klene, X. Li, J.E. Knox, H.P. Hratchian, J.B. Cross, C. Adamo, J. Jaramillo, R. Gomperts, R.E. Stratmann, O. Yazyev, A.J. Austin, R. Cammi, C. Pomelli, J.W. Ochterski, P.Y. Ayala, K. Morokuma, G.A. Voth, P. Salvador, J.J. Dannenberg, V.G. Zakrzewski, S. Dapprich, A.D. Daniels, M.C. Strain, O. Farkas, D.K. Malick, A.D. Rabuck, K. Raghavachari, J.B. Foresman, J.V. Ortiz, Q. Cui, A.G. Baboul, S. Clifford, J. Cioslowski, B.B. Stefanov, G. Liu, A. Liashenko, P. Piskorz, I. Komaromi, R.L. Martin, D.J. Fox, T. Keith, M.A. Al-Laham, C.Y. Peng, A. Nanayakkara, M. Challacombe, P.M.W. Gill, B. Johnson, W. Chen, M.W. Wong, C. Gonzalez, J.A. Pople, Gaussian 03, Revision B.01, Gaussian Inc, Pittsburgh, PA, 2003.
[24] B. Droźdź, M. Holub, Z. Samek, V. Herout, F. Šorm, Coll. Czech. Chem. Commun. 33 (1968) 1730–1737.
[25] F. Chain, E. Romano, P. Leyton, C. Paipa, C.A.N. Catalán, M.A. Fortuna, S.A. Brandán, J. Mol. Struct. 1065–1066 (2014) 160–169.
[26] E.D. Glendening, J.K. Badenhoop, A.D. Reed, J.E. Carpenter, F. Weinhold, NBO 3.1; Theoretical Chemistry Institute, University of Wisconsin, Madison, WI, 1996.
[27] B.H. Besler, K.M. Merz Jr, P.A. Kollman, J. Comp. Chem. 11 (1990) 431–439.
[28] G. Rauhut, P. Pulay, J. Phys. Chem. 99 (1995) 3093–3100.
[29] T. Sundius, Scaling of ab-initio force fields by MOLVIB, Vib. Spectrosc. 29 (2002) 89–95.
[30] T. Sundius, J. Mol. Struct. 218 (1990) 321–326.
[31] R. Ditchfield, Mol. Phys. 27 (1974) 789–807.
[32] J. Cheeseman, G. Trucks, T. Keith, M. Frisch, J. Chem. Phys. 104 (1996) 5497–5509.
[33] T.A. Keith, R.F.W. Bader, Chem. Phys. 210 (1993) 223–231.
[34] A. Esmaeili, N. Moazami, A. Rustaiyan, Pakistan, J. Pharm. Sci. 25 (1) (2012) 155–159.
[35] G. Keresztury, S. Holly, G. Besenyei, J. Varga, A. Wang, J.R. Durig, Spectrochim. Acta 49A (1993) 2007.
[36] G. Keresztury, J.M. Chalmers, P.R. Griffith (Eds.), Raman spectroscopy: theory, in hand book of vibrational spectroscopy, vol. 1, John Wiley & Sons Ltd., New York, 2002.
[37] A.B. Brizuela, A.B. Raschi, M.V. Castillo, P. Leyton, E. Romano, S.A. Brandán, Comput. Theor. Chem. 1008 (2013) 52–60.
[38] O.E. Piro, G.A. Echeverría, E. Lizárraga, E. Romano, C.A.N. Catalán, S.A. Brandán, Spectrochim. Acta Part A 101 (2013) 196–203.
[39] E. Romano, J.L. Pergomet, J. Zinczuk, S.A. Brandán, Structural and Vibrational Properties of some quinoline acetic acid derivatives with potentials biological activities. Acetic Acids: Chemical Properties, Production and Applications, Edited Collection, Nova Science Publishers, 2013.
[40] R.G. Parr, R.G. Pearson, J. Am. Chem. Soc. 105 (1983) 7512–7516.
[41] P.K. Chattaraj, D.R. Roy, S. Giri, S. Mukherjee, V. Subramanian, R. Parthasarathi, P. Bultinck, S.J. Van Damme, Chem. Sci. 119 (5) (2007) 475–488.
[42] M.B. Márquez, S.A. Brandán, Int. J. Quant. Chem. 114 (3) (2014) 209–221.